J. Fluid Mech. (1985), *vol.* 156, *pp.* 479–494
Printed in Great Britain

The inertial draining of a thin fluid layer between parallel plates with a constant normal force. Part 2. Boundary layer and exact numerical solutions

By C. J. LAWRENCE, Y. KUANG AND S. WEINBAUM
Department of Mechanical Engineering, The City College of The City University of New York, New York, New York 10031

(Received 11 October 1984 and in revised form 30 January 1985)

The draining of a fluid layer between rigid plane parallel boundaries under a constant normal force is considered. In Part 1 the effect of fluid inertia was considered in the inviscid and low- but finite-Reynolds-number limits along with the inertia of the moving body; in Part 2, we consider the case of negligible inertia of the moving body. We develop an approximate large-Reynolds-number solution, valid until the boundary layers of the rigid surfaces begin to overlap, and present a new exact solution of the full Navier–Stokes equations for a time-dependent double-axisymmetric stagnation-point flow. These solutions exhibit interesting new features that illustrate the coupling of a time-dependent inviscid core flow with the growth of an unsteady boundary layer started from rest and the effect of Reynolds number on the merging of the boundary layers at large time.

1. Introduction

The general problem of the combined inertial and viscous draining of a fluid between rigid parallel surfaces under the action of a constant applied force such as gravity was formulated and various limiting behaviours defined in Part 1 (Weinbaum, Lawrence & Kuang 1985). The geometry and coordinate system are shown in figure 1. It was shown that the motion of the fluid and the pressure distribution in the thin fluid gap between the two rigid surfaces and away from edge effects had several simplifying features. The radial dependence of the velocity field and pressure distribution could be determined independent of Reynolds number and the Navier–Stokes equations reduced to a single nonlinear partial differential equation containing two dimensionless parameters based on the characteristic timescales of the problem. There are four major contributions to the force balance on the moving body. The first is the net external force, including buoyancy, which can be scaled to unity leaving three dimensionless forces describing the inertial contribution of the body, the inertial contribution of the fluid and the viscous contribution of the fluid. These forces are associated with three characteristic timescales: the gravitational time t_g is the time for the body to fall under the action of the net external force and its own inertia; the inertial time t_i is the time for the fluid to drain under the action of the external force and the fluid inertia; and the viscous diffusion time t_d is the time for the vorticity generated at the two boundaries to spread through the initial gap height. The three times give rise to the two parameters, the Reynolds number $Re = t_d/t_i$ and $\beta = t_g^2/t_i^2$. A fourth timescale is the viscous flow time t_v; it characterizes the time for the body to fall in the absence of inertia. It is not independent of the others since $t_v = t_i^2/t_d$.

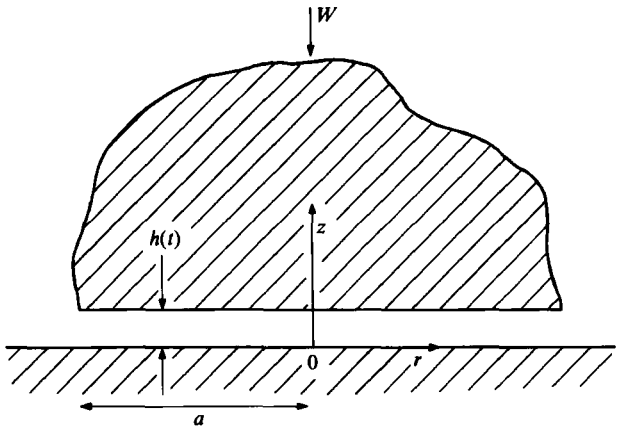

FIGURE 1. Sketch of the geometry showing the coordinate axes.

In this paper, we will deal exclusively with the case when $\beta = 0$, that is the limit which the inertial time is much longer than the gravitational time. In this limit the external force is always balanced by the hydrodynamic force and the inertia of the moving body is neglected. The necessary conditions for this to occur have already been discussed in Part 1, and analytical solutions for small but finite *Re* presented. With $\beta = 0$, the differential equation can be solved numerically for all Reynolds numbers. This constitutes an exact numerical solution of the full Navier–Stokes equations, in the sense that the radial dependence of the velocity field is found analytically before solving for the time and axial dependence, and all nonlinear terms are retained in the solution. Two approximate solutions are also presented herein, one for large Reynolds numbers and one for short times for all *Re*. The large-Reynolds-number solution is an extension of the infinite *Re* inviscid solution developed in Part 1 to the case of thin boundary layers at large but finite *Re*. A novel split-profile integral-equation technique is used to obtain a solution which is valid up to the time when the two boundary layers meet. The small-time solution is developed to avoid the singular behaviour in the growth of the boundary-layer thickness at very early times.

2. Formulation

In Part 1 (Weinbaum, Lawrence & Kuang 1985) it was shown that the Navier–Stokes equations for this problem reduce to a single equation for the axial- and time-dependent reduced stream function $F(z,t)$. In the limit where the rate of change of body momentum is negligible ($\beta = 0$) the differential equation for F when rendered dimensionless simplifies to

$$F_{zt} + F_z^2 - 2FF_{zz} - \frac{t_c}{t_i}\frac{1}{Re}F_{zzz} = \frac{t_c^2}{t_i^2}, \tag{1}$$

in which t_c is the characteristic time used in the non-dimensionalization, t_i is the characteristic inertial time of the problem $t_i = (\pi\rho a^4/4W)^{\frac{1}{2}}$ and *Re* is a Reynolds number, the ratio of the characteristic viscous time $t_d = h_0^2/\nu$ to the inertial time t_i, i.e. $Re = t_d/t_i$. The stream function is $\psi = r^2F$, with velocity components $u = rF_z$ and $w = -2F$.

The boundary and initial conditions for (1) are

$$F = 0 \quad \text{and} \quad F_z = 0 \quad \text{on} \quad z = 0, \tag{2a,b}$$

$$F = -\tfrac{1}{2}h_t \quad \text{and} \quad F_z = 0 \quad \text{on} \quad z = h(t), \tag{3a,b}$$

$$F = 0 \quad \text{and} \quad h = 1 \quad \text{when} \quad t = 0. \tag{4a,b}$$

Equation (3*a*) is a second equation coupling the two dependent variables $F(z,t)$ and $h(t)$. Equation (1) is a nonlinear partial differential equation with nonlinear boundary conditions and as such must be solved numerically in the general case. The numerical solution is presented here, together with the two limiting cases (i) small $t, h \approx 1$, (ii) large Re. The near-lubrication case of small Re was discussed in Part 1.

3. Small-time solution

An asymptotic solution can be found for the short period after the release of the body when it remains close to its original position. This solution is useful in starting the longer-time solutions in the following sections and is an interesting exercise in asymptotic analysis. To reveal the behaviour for short times, t_c is chosen to be ϵt_1 with ϵ a small constant. New symbols are introduced for the dimensionless variables: τ for time and G for stream function. The boundary and initial conditions are unchanged and (1) is re-written as

$$G_{z\tau} + G_z^2 - 2GG_{zz} = \epsilon \frac{1}{Re} G_{zzz} + \epsilon^2. \tag{5}$$

The required solution must be asymptotic for fixed z and Re as $\epsilon \to 0$. A suitable form is

$$G(z,\tau;\epsilon) \sim \epsilon^2 G_4(z,\tau) + \epsilon^{\frac{5}{2}} G_5(z,\tau) + O(\epsilon^3). \tag{6}$$

Equations for G_4 and G_5 are found by substituting (6) into (5):

$$G_{4z\tau} = 1, \tag{7}$$

$$G_{5z\tau} = 0. \tag{8}$$

Equations (7) and (8) have solutions

$$G_4 = z\tau + a_4(\tau) + b_4(z), \tag{9}$$

$$G_5 = a_5(\tau) + b_5(z), \tag{10}$$

where a_4, b_4, a_5 and b_5 are unknown functions. Initial condition (4*a*) requires that $b_4 = b_5 = 0$, but the boundary conditions (2) and (3) cannot be satisfied by (9) and (10). Therefore, boundary layers must be present near $z = 0$ and 1, so inner expansions must be used. To examine the boundary layer near $z = 0$, z is replaced by a new independent variable $\zeta = z/\epsilon^{\frac{1}{2}}$ and G is replaced by $g = G/\epsilon^{\frac{5}{2}}$. Equation (5) takes the form

$$g_{\zeta\tau} - \frac{1}{Re} g_{\zeta\zeta\zeta} - 1 = \epsilon^2 (2g_{\zeta\zeta} - g_\zeta^2). \tag{11}$$

The solution to (11) must be asymptotic for fixed ζ and Re as $\epsilon \to 0$, in the form

$$g(\zeta,\tau;\epsilon) \sim g_0(\zeta,\tau) + O(\epsilon^{\frac{1}{2}}). \tag{12}$$

This expansion (12) is substituted into (11) to give an equation for g_0

$$g_{0\zeta\tau} - \frac{1}{Re} g_{0\zeta\zeta\zeta} - 1 = 0. \tag{13}$$

Note that (13) is the same as the start-up problem for unidirectional flow in a channel under the action of a constant applied pressure gradient. The boundary and initial conditions for g_0 are:

$$g_0 = 0, \quad g_{0\zeta} = 0 \quad \text{on} \quad \zeta = 0; \quad \text{and} \quad g_0 = 0 \quad \text{when} \quad t = 0. \tag{14}$$

Equations (13) and (14) have a solution in similarity form

$$g_0 = \zeta\tau + \frac{8}{Re^{\frac{1}{2}}} \tau^{\frac{3}{2}} \left\{ \mathrm{i}^3 \operatorname{erfc}\left[\frac{\zeta}{2} \left(\frac{Re}{\tau} \right)^{\frac{1}{2}} \right] - \frac{1}{6\pi^{\frac{1}{2}}} \right\}, \tag{15}$$

where i^3 erfc is the third repeated integral of the complementary error function, which takes the value $1/6\pi^{\frac{1}{2}}$ for zero argument.

It is expected that G will be of order ϵ^2 everywhere, so boundary condition (3a) suggests that h will be of the form

$$h(\tau; \epsilon) \sim 1 + \epsilon^2 h_4(\tau) + \epsilon^{\frac{5}{2}} h_5(\tau) + O(\epsilon^3). \tag{16}$$

Relation (16) indicates that the upper boundary will move very little from its initial position during the timescale of interest. Accordingly, boundary conditions (3) can be expanded in Taylor series about $z = 1$ to give conditions applicable at $z = 1$ and the appropriate boundary-layer variable is $\xi = (1-z)/\epsilon^{\frac{1}{2}}$. Equation (7) is rewritten in terms of ξ and a scaled stream function $\tilde{g} = G/\epsilon^{\frac{5}{2}}$ to give

$$\tilde{g}_{\xi\tau} - \frac{1}{Re} \tilde{g}_{\xi\xi\xi} = -1 - \epsilon^2 (2\tilde{g}\tilde{g}_{\xi\xi} - \tilde{g}_{\xi}^2). \tag{17}$$

The required solution to (17) is asymptotic for fixed ξ and Re as $\epsilon \to 0$ and in the form

$$\tilde{g}(\xi, \tau; \epsilon) \sim \epsilon^{-\frac{1}{2}} \tilde{g}_{-1}(\xi, \tau) + \tilde{g}_0(\xi, \tau) + O(\epsilon^{\frac{1}{2}}). \tag{18}$$

(18) is inserted into (17) to give equations for $\tilde{g}_{-1}$ and $\tilde{g}_0$:

$$\tilde{g}_{-1\xi\tau} - \frac{1}{Re} \tilde{g}_{-1\xi\xi\xi} = 0; \tag{19}$$

$$\tilde{g}_{0\xi\tau} - \frac{1}{Re} \tilde{g}_{0\xi\xi\xi} + 1 = 0, \tag{20}$$

with boundary and initial conditions derived from (3) and (4):

$$\tilde{g}_{-1\xi} = 0, \quad \tilde{g}_{-1} = -\tfrac{1}{2} h_{4\tau} \quad \text{on} \quad \xi = 0 \quad \text{and} \quad \tilde{g}_{-1} = 0 \quad \text{when} \quad \tau = 0; \tag{21}$$

$$\tilde{g}_{0\xi} = 0, \quad \tilde{g}_0 = -\tfrac{1}{2} h_{5\tau} \quad \text{on} \quad \xi = 0 \quad \text{and} \quad \tilde{g}_0 = 0 \quad \text{when} \quad \tau = 0. \tag{22}$$

Equations (19) to (22) are solved to find

$$\tilde{g}_{-1} = -\tfrac{1}{2} h_{4\tau}, \tag{23}$$

and

$$\tilde{g}_0 = -\tfrac{1}{2} h_{5\tau} - \xi\tau - \frac{8}{Re^{\frac{1}{2}}} \tau^{\frac{3}{2}} \left\{ \mathrm{i}^3 \operatorname{erfc}\left[\frac{\xi}{2} \left(\frac{Re}{\tau} \right)^{\frac{1}{2}} \right] - \frac{1}{6\pi^{\frac{1}{2}}} \right\}. \tag{24}$$

Expansions (6), (12) and (18) are matched on intermediate spatial scales to give equations for a_4, a_5, b_4, b_5, h_4 and h_5. These are:

$$a_4(\tau) = 0, \quad a_5(\tau) = -\frac{4}{3\pi^{\frac{1}{2}}}\tau^{\frac{3}{2}}Re^{-\frac{1}{2}}; \tag{25}$$

$$b_4(z) = 0, \quad b_5(z) = 0; \tag{26}$$

$$h_{4\tau} = -2\tau, \quad h_{5\tau} = -2a_5 + \frac{8}{3\pi^{\frac{1}{2}}}\tau^{\frac{3}{2}}Re^{-\frac{1}{2}}. \tag{27}$$

Equations (27) with initial condition (4*b*) have solutions

$$h_4 = -\tau^2, \tag{28}$$

$$h_5 = \frac{32}{15\pi^{\frac{1}{2}}}\tau^{\frac{5}{2}}Re^{-\frac{1}{2}}. \tag{29}$$

Finally, we have a uniform asymptotic expansion for G,

$$G \sim \epsilon^2 z\tau - 8\epsilon^{\frac{5}{2}}\tau^{\frac{3}{2}}Re^{-\frac{1}{2}}\left\{\frac{1}{6\pi^{\frac{1}{2}}} - \mathrm{i}^3\,\mathrm{erfc}\left(\frac{z}{2}\left(\frac{Re}{\epsilon\tau}\right)^{\frac{1}{2}}\right) + \mathrm{i}^3\,\mathrm{erfc}\left[\frac{1-z}{2}\left(\frac{Re}{\epsilon\tau}\right)^{\frac{1}{2}}\right]\right\} + O(\epsilon^3), \tag{30}$$

and

$$h \sim 1 - \epsilon^2\tau^2 + \frac{32}{15\pi^{\frac{1}{2}}}Re^{-\frac{1}{2}}\epsilon^{\frac{5}{2}}\tau^{\frac{5}{2}} + O(\epsilon^3). \tag{31}$$

Equations (5), (11) and (17) show that no more terms will be generated until $O(\epsilon^4)$, so the remainder terms in (30) and (31) can be reduced. Since ϵ was artificially introduced into the problem, it can be removed by using a different timescale to express the results. If t_c is chosen to be t_1, as will be the case in the rest of this paper, the expansions are expressed in their most useful form:

$$F \sim zt - 8t^{\frac{3}{2}}Re^{-\frac{1}{2}}\left[\frac{1}{6\pi^{\frac{1}{2}}} - \mathrm{i}^3\,\mathrm{erfc}\left(\frac{z}{2}\left(\frac{Re}{t}\right)^{\frac{1}{2}}\right) + \mathrm{i}^3\,\mathrm{erfc}\left(\frac{1-z}{2}\left(\frac{Re}{t}\right)^{\frac{1}{2}}\right)\right] + O(t^3); \tag{32}$$

$$h \sim 1 - t^2 + \frac{32}{15\pi^{\frac{1}{2}}}Re^{-\frac{1}{2}}t^{\frac{5}{2}} + O(t^4). \tag{33}$$

These expansions are valid whenever $t \ll 1$ and $t \ll Re$. The velocity profile is

$$\frac{u}{r} \sim t\left\{1 - 4\mathrm{i}^2\,\mathrm{erfc}\left(\frac{z}{2}\left(\frac{Re}{t}\right)^{\frac{1}{2}}\right) - 4\mathrm{i}^2\,\mathrm{erfc}\left[\frac{1-z}{2}\left(\frac{Re}{t}\right)^{\frac{1}{2}}\right]\right\} + O(t^3). \tag{34}$$

Expansion (34) shows a uniform constant acceleration in the inviscid core with boundary layers whose thickness grows as $(t/Re)^{\frac{1}{2}}$. For small Re the above expansions quickly become invalid as the boundary layers merge and viscous effects dominate the flow. For large Reynolds numbers the boundary layers persist for a long time but the expansions break down when nonlinear effects become important and the acceleration is no longer constant. The effect of Re first enters in terms of $O(\epsilon^{\frac{5}{2}})$ in (31) or (33) and describes the radial outflow in the top and bottom start-up boundary layers for a uniformly accelerated core.

4. Solution for large Re

When the Reynolds number is large, the flow is governed by the inertia of the fluid except for thin boundary layers near the top and bottom walls. Thus, it is appropriate to choose the characteristic inertial time $t_c = t_i$ in (1). This gives

$$F_{zt} + F_z^2 - 2FF_{zz} - \frac{1}{Re} F_{zzz} = 1. \tag{35}$$

Equations (35) and (3a) must be satisfied in the inviscid core. In this region the reduced stream function F takes the simpler form

$$F = z\Phi(t) + \Theta(t), \tag{36}$$

where the first term describes an inviscid stagnation-point flow and the second term, as we shall soon show, the displacement effect of the boundary layers. Substituting (36) in (35), one obtains

$$\Phi^2 + \Phi_t = 1. \tag{37a}$$

Φ and Θ satisfy the initial conditions

$$\Phi = 0, \quad \Theta = 0 \quad \text{when} \quad t = 0. \tag{37b,c}$$

Equations (37a) and (37b) have the solution

$$\Phi = \tanh t. \tag{38}$$

This is the same as (33) of Part 1 (Weinbaum *et al.* 1985), which is the solution in the inviscid limit. Boundary conditions (2b) and (3b) cannot be satisfied by (36), so it is necessary to consider boundary layers near $z = 0$ and $z = h(t)$. The radial velocity outside the boundary layers near $z = 0$ and $z = h(t)$. The radial velocity outside the boundary layers is determined by the radial pressure gradient alone and is simply $u = r \tanh t$. It is unaffected by the presence of the boundary layers, so the analysis will be valid until the boundary layers overlap.

To analyse the boundary layer near $z = 0$, new variables $\zeta = z\,Re^{\frac{1}{2}}$ and $f = F\,Re^{\frac{1}{2}}$ are introduced. Equation (35) becomes the boundary-layer equation

$$f_{\zeta t} + f_\zeta^2 - 2ff_{\zeta\zeta} - f_{\zeta\zeta\zeta} = 1, \tag{39}$$

which has initial and boundary conditions

$$f = 0 \quad \text{when} \quad t = 0, \tag{40}$$

$$f = 0, \quad f_\zeta = 0 \quad \text{on} \quad \zeta = 0, \tag{41a,b}$$

$$f \sim \zeta\Phi - Re^{\frac{1}{2}}\Theta \quad \text{as} \quad \zeta \to \infty. \tag{42}$$

In (36), Θ is the correction to the inviscid vertical velocity due to the displacement effect of the boundary layers. To illustrate this, the boundary-layer displacement thickness δ^* is introduced:

$$\delta^*(t) = Re^{-\frac{1}{2}} \int_0^\infty \left(1 - \frac{f_\zeta}{\Phi}\right) \mathrm{d}\zeta = Re^{-\frac{1}{2}} \Delta^*, \tag{43}$$

in which f_ζ and Φ respectively represent the radial velocity in the boundary layer and core, and Δ^* is of order unity. Equation (43) is integrated directly and (42) is used to obtain

$$\delta^*(t) = \frac{\Theta(t)}{\Phi(t)} \quad \text{or} \quad \Theta(t) = \delta^*(t)\,\Phi(t). \tag{44a,b}$$

Then in terms of δ^*, the stream function in the inviscid core is

$$F = (z-\delta^*)\,\Phi, \tag{45}$$

and the limiting condition on the boundary-layer equation (42) becomes

$$f \sim (\zeta-\Delta^*)\,\Phi \quad \text{as} \quad \zeta \to \infty. \tag{46}$$

The flow is clearly symmetrical about the plane $z = \frac{1}{2}h$, so the boundary-layer equations on the top surface $z = h$ can be cast in the same form as (39), (40), (41) and (46). To achieve this, new variables, $\tilde{\zeta} = Re^{\frac{1}{2}}(h-z)$ and $\tilde{f} = Re^{\frac{1}{2}}[\Phi h - F - 2\Theta]$, are introduced and substituted into (35), (3) and (4a). The resulting equations are then separated in powers of Re to give the same set of boundary-layer equations, but with $\tilde{f}$ and $\tilde{\zeta}$ replacing f and ζ. However a new equation is also produced from (3a) and (45),

$$h_t + 2h\Phi - 4\Theta = 0. \tag{47}$$

Using initial condition (4b), one can solve equation (47) exactly to give

$$h = \frac{1}{\cosh^2 t} + Re^{-\frac{1}{2}} h_1(t), \tag{48}$$

in which $h_1(t)$ is the correction to the inviscid result due to the displacement effect of the boundary layers. It satisfies the equations

$$h_{1t} + 2(h_1 - 2\Delta^*)\,\Phi = 0, \tag{49}$$

$$h_1 = 0 \quad \text{when} \quad t = 0. \tag{50}$$

Equations (36), (39)–(41), (46) and (48)–(50) represent a solution which is exact whenever there are distinct boundary layers in the flow. The solution only breaks down when the boundary layers begin to overlap. $\delta^*(t)$ represents the correction to the inviscid solution developed in Part 1 (Weinbaum *et al.* 1985). It is determined by solving (39)–(41) and (46) and can then be used in (49) to calculate the correction to the gap height, $h_1(t)$. It is possible to solve (39) numerically, but this is complicated by the presence of the time derivative and is tantamount to a solution of the full Navier–Stokes equation which is undertaken in §5 below. To gain from a boundary-layer analysis we must simplify the equation, so we will find an approximate solution using a time-dependent momentum-integral method.

Equation (39) is reduced to an ordinary differential equation by integrating through the boundary layer and assuming a particular form for the velocity profile. A new variable, $\delta(t) = Re^{\frac{1}{2}}\Delta(t)$ is introduced to represent the outer edge of the boundary layer. Equation (39) is integrated over ζ from 0 to Δ to give

$$[f(\Delta)]_t - \Delta_t f_\zeta(\Delta) + 3\int_0^\Delta f_\zeta^2\,\mathrm{d}\zeta - 2f_\zeta(\Delta)\,f(\Delta) - f_{\zeta\zeta}(\Delta) + f_{\zeta\zeta}(0) - \Delta = 0, \tag{51}$$

where $f(\Delta)$ is an abbreviation for $f(\Delta(t), t)$ etc.

A bi-quadratic radial-velocity profile is chosen ($u = rf_\zeta$) where the velocity and its gradient are matched at $\zeta = k\Delta$. A simple cubic or quartic profile is not sufficiently general to describe the behaviour at early time:

$$f = a_0 + a_1\zeta + a_2\zeta^2 + a_3\zeta^3, \quad 0 \leqslant \zeta \leqslant k\Delta; \tag{52a}$$

$$f = b_0 + b_1\zeta + b_2\zeta^2 + b_3\zeta^3, \quad k\Delta \leqslant \zeta \leqslant \Delta. \tag{52b}$$

The a_i and b_i and δ are functions of t, but k is a constant to be chosen at a later stage in the analysis. The boundary conditions to be satisfied by (52) are:

$$f = 0, \quad f_\zeta = 0, \quad f_{\zeta\zeta\zeta} = -1 \quad \text{on} \quad \zeta = 0; \tag{53a,b,c}$$

$$f_\zeta = \Phi, \quad f_{\zeta\zeta} = 0 \quad \text{on} \quad \zeta = \Lambda; \tag{54a,b}$$

$$f, f_\zeta \text{ and } f_{\zeta\zeta} \quad \text{continuous on} \quad \zeta = k\Lambda. \tag{55a–c}$$

Equations (53a, b) are the original boundary conditions; (53c) is derived by setting $\zeta = 0$ in (39). Equations (54) constitute the definition of the outer edge of the boundary layer and (55) are desirable smoothness properties of the velocity profile. Equations (52)–(55) are solved to find the coefficients a_i and b_i in terms of the still unknown k and $\Lambda(t)$:

$$a_0 = 0, \quad a_1 = 0, \quad a_2 = \frac{k\Lambda^2 + 2\Phi}{2\Lambda(1+k)}, \quad a_3 = -\tfrac{1}{6}; \tag{56}$$

$$b_0 = \frac{-k^3\Lambda(\Lambda^2 - 2\Phi)}{6(1-k^2)}, \quad b_1 = \frac{k^2(\tfrac{1}{2}\Lambda^2 - \Phi)}{(1-k^2)}, \quad b_2 = \frac{\Phi - \tfrac{1}{2}k^2\Lambda^2}{\delta(1-k^2)}, \quad b_3 = \frac{k^2\Lambda^2 - 2\Phi}{6\Lambda^2(1-k^2)}. \tag{57}$$

Equations (52), (56) and (57) describe a family of velocity profiles which, once k is chosen, will have a single parameter, $\Lambda(t) = \Lambda^2/\Phi$. These equations are substituted into (51) and after a great deal of algebraic manipulation an equation for Λ is derived:

$$\Lambda_t = \frac{-1 + \Lambda[\tfrac{1}{2} + d_1\Phi_t + d_2\Phi^2] + \Lambda^2[-\tfrac{1}{8}k^2\Phi_t + d_3\Phi^2] + \Lambda^3 d_4\Phi^2}{\Phi(\tfrac{1}{8}k^2\Lambda + d_5)}, \tag{58}$$

where $d_1, \ldots, d_5$ are constants depending only on the choice of k. If a simple cubic or quartic profile had been used one would obtain in place of (58) an equation with no real roots for Λ at $t = 0$:

$$d_1 = \tfrac{1}{4}(k^2 - k - 1); \quad d_2 = -\tfrac{1}{3}(k^2 - 2k - 2) + \frac{2}{5}\frac{2k^3 - k^2 - 4k - 2}{1+k}; \tag{59a,b}$$

$$d_3 = \tfrac{1}{6}k^2 - \tfrac{1}{20}k^2\frac{k^3 - 3k^2 + 8k + 4}{1+k}; \tag{59c}$$

$$d_4 = \tfrac{1}{40}k^4\frac{k-3}{1+k}; \quad d_5 = -\tfrac{1}{12}(k^2 - 5k - 5). \tag{59d,e}$$

Before an attempt is made to solve (58), it is useful to consider the range of values for Λ. The shear stress must be positive in the boundary layer, which requires that $f_{\zeta\zeta} \geqslant 0$ everywhere. This is true only for values of Λ between $\Lambda_{\min} = -2/k$ and $\Lambda_{\max} = 2/k^2$, so Λ is bounded. Furthermore, Λ must be positive since Φ is always positive. Thirdly, there is a value Λ_b for which the denominator of (58) vanishes and the profile shape changes discontinuously. This non-physical behaviour is not permissible and occurs when

$$\Lambda = \Lambda_b = \frac{2}{3k^2}(k^2 - 5k - 5). \tag{60}$$

We can also use (58) to find the initial and final values for Λ. For very large time, the flow in the boundary layer will be that for a quasi-steady stagnation point, since Φ from (38) approaches unity and Λ will approach a steady value Λ_∞ which satisfies

$$d_4\Lambda_\infty^3 + d_3\Lambda_\infty^2 + d_2\Lambda_\infty - 1 = 0. \tag{61}$$

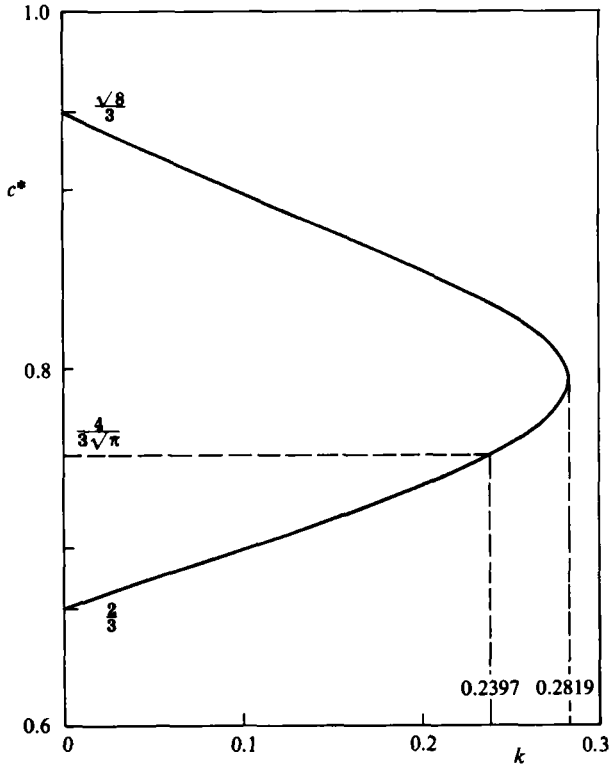

FIGURE 2. Variation of the coefficient c^* with choice of k.

When $t = 0$, the denominator of (58) vanishes since Φ is zero. Since A should not be singular, the numerator must also vanish. One can show that the vanishing of the numerator requires that A have the initial value A_0, with

$$A_0 = \frac{1}{k^2}\{(1-k+k^2) \pm [(1-k+k^2)^2 - 8k^2]^{\frac{1}{2}}\}, \tag{62}$$

using the fact that $\Phi \sim t$ at very short time. Equation (62) can be used to find a suitable value for k since the analytic solution is available for the first part of the motion. Equations (32) and (46) imply that when t is small $\Delta^* = (4/3\pi^{\frac{1}{2}})\, t^{\frac{1}{2}}$. For the assumed velocity profile (52), the scaled displacement thickness is

$$\Delta^* = \Delta \frac{(1+k+k^2) - \frac{1}{2}k^2 A}{3(1+k)}. \tag{63}$$

From the definition of A, $\Delta = A^{\frac{1}{2}} \Phi^{\frac{1}{2}}$ and so, when t is small,

$$\Delta \sim A_0^{\frac{1}{2}}\, t^{\frac{1}{2}}. \tag{64}$$

Equation (64) is substituted into (63) to give for small t

$$\Delta^* = c^* t^{\frac{1}{2}}, \tag{65}$$

with

$$c^* = A_0^{\frac{1}{2}} \frac{(1+k+k^2) - \frac{1}{2}k^2 A_0}{3(1+k)}. \tag{66}$$

For each value of k, (62) and (66) give two values of c^* (one for each root of A_0), as shown in figure 2. There are no real solutions for c^* if k is chosen larger than 0.2819.

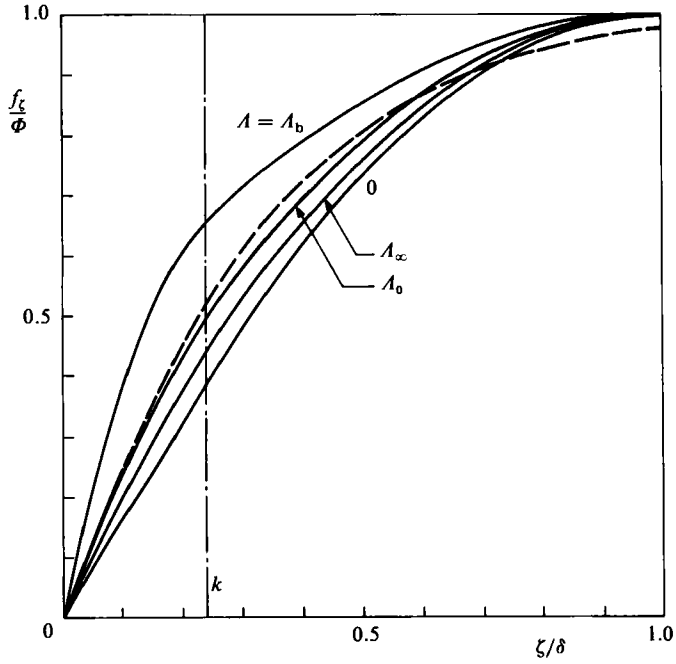

FIGURE 3. Velocity profiles in the boundary layer: ——, biquadratic profiles used in integral solution (53), ($k = 0.2397$, $\Lambda_0 = 6.2745$, $\Lambda_\infty = 3.0315$, $\Lambda_b = 15.05$); – – – –, analytic solution for small t (34).

This means that, for larger k, the velocity profile (52) is not an adequate representation of the true solution and leads to physically unrealizable results. For k smaller than this limit, values of c^* between $\frac{2}{3}$ and $\frac{2\sqrt{2}}{3}$ are physically possible. However, if we wish to obtain limiting behaviour for δ^* at very short times, which is the same as the analytic solution in §3, then c^* must be $4/3\pi^{\frac{1}{2}}$. This corresponds to the value of $k = 0.2397$ which is on the lower branch of the curve using the negative sign in (62). With this value of k, equations (60)–(62) give

$$\Lambda_0 = 6.275, \quad \Lambda_\infty = 3.032, \quad \Lambda_b = 15.05. \tag{67}$$

The shape of the velocity profile is shown in figure 3 for these values of Λ and for $\Lambda = 0$. It is clear that very little change in the profile occurs between the values Λ_0 and Λ_∞. The small-time profile (34) is drawn on a corresponding scale and we see that it is modelled quite closely by the curve for Λ_0.

Equation (58) is relatively easy to integrate numerically to find $\Lambda(t)$, $\delta(t)$ and $\delta^*(t)$, which are shown in figure 4. Λ decays monotonically from Λ_0 to Λ_∞ and is well within the physical bounds defined above. δ and δ^* do not increase monotonically, but increase to maxima just after $t = 1$ and then decay slightly to their steady values. The steady value of δ^* is $0.5665\,Re^{-\frac{1}{2}}$, which compares well with the exact numerical solution for steady stagnation-point flow obtained by Frössling (1940) $\delta^* = 0.5685\,Re^{-\frac{1}{2}}$. The decline in δ and δ^* can be explained by regarding the end of the boundary-layer development as a quasi-steady stagnation-point flow. For the steady flow the boundary-layer thickness is inversely proportional to the square root of the core velocity. Thus, as the velocity increases slowly towards its steady value, the boundary-layer thickness decreases slightly. The steady value of δ, $1.741\,Re^{-\frac{1}{2}}$, can be used to estimate the limit of validity of the solution. When Re is sufficiently

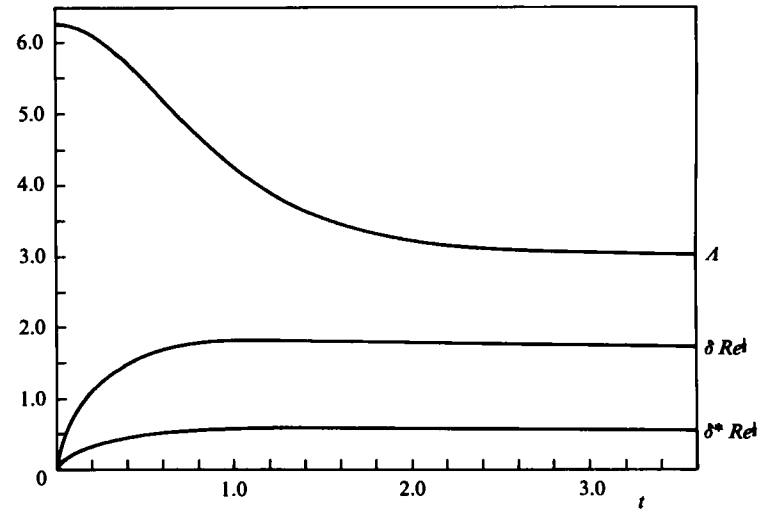

FIGURE 4. Numerical solution of (58) for $A(t)$, $\delta(t)$ and $\delta^*(t)$.

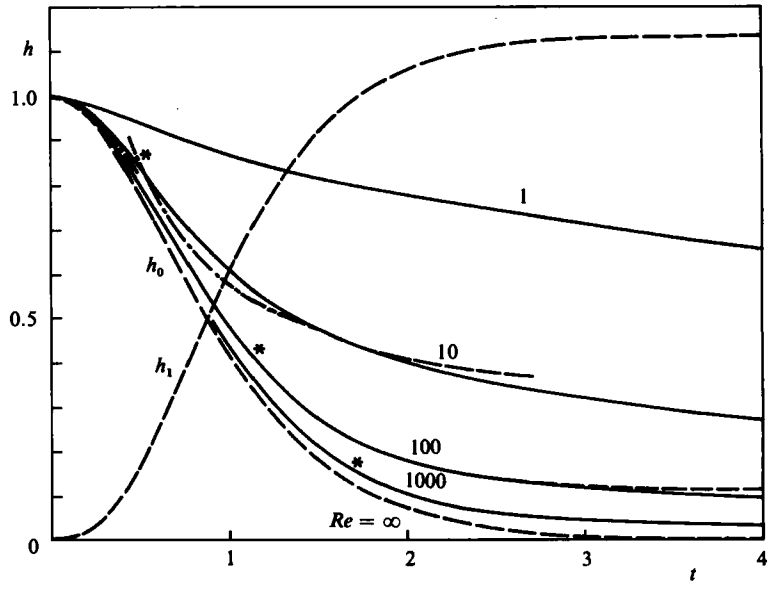

FIGURE 5. Solutions for the gap height $h(t)$: ——, numerical solution; – – – –, integral boundary-layer solution for large Re (h_0, h_1 also shown); *, predicted limit of validity of large Re solution; –·–·–·–, matched asymptotic solution for small Re.

large, the steady-state boundary layer will develop before the limit is reached and $h(t)$ is accurately approximated by $1/\cosh^2 t$. The limit is reached when $h = 2\delta \approx 3.5\,Re^{-\frac{1}{2}}$; this gives the limit of validity, $t_{\max} \sim \frac{1}{4}\log Re$.

Equations (49) and (50) are integrated numerically using the solution for δ^*. The displacement correction to the inviscid solution for the gap height h_1 is shown in figure 5 together with the total height for various Reynolds numbers. These solutions have the limit of validity derived above; after the limit is passed the height tends to a constant non-zero value, which is not physically possible. However, for $Re > 10^4$,

the body falls through more than 98 % of the initial height before the limit is reached, so the approximate solution describes the important part of the motion.

It will be shown that the solutions are very accurate compared with the exact numerical solution until the limit derived above is reached. The two important features of the solution which give rise to this accuracy are the use of the analytically derived form for δ^* when t is small and the fact that the radial velocity component in the inviscid core is independent of the displacement effect of the top and bottom boundary layers.

5. Numerical solution

The boundary conditions (3) at the moving boundary $z = h$ are inconvenient to apply in a numerical solution, so a new independent variable $x = z/h(t)$ is introduced. The characteristic inertial time t_i is used for non-dimensionalization, since it is the time most commonly used in the previous sections. For brevity, the velocity $U = (1/h)F_x$ is introduced and (1) becomes

$$U_t + U^2 - \frac{2FU_x}{h} - \frac{xh_t U_x}{h} - \frac{U_{xx}}{Re\,h^2} - 1 = 0. \tag{68}$$

Equation (68) contains a new term arising from the time dependence of the x-coordinate.

The boundary conditions become:

$$F = 0, \quad U = 0 \quad \text{on} \quad x = 0; \tag{69}$$

$$F = -\tfrac{1}{2}h_t, \quad U = 0 \quad \text{on} \quad x = 1. \tag{70}$$

The flow is symmetrical about $x = \frac{1}{2}$, so the equation need be solved only in the region $0 \leqslant x \leqslant \frac{1}{2}$ and (70) can be replaced by

$$F = -\tfrac{1}{4}h_t, \quad U_x = 0 \quad \text{on} \quad x = \tfrac{1}{2}. \tag{71}$$

Equations (68), (69) and (71) are solved using an implicit central-difference numerical scheme. For small to moderate Re, the boundary-layer development is so rapid that no special consideration is needed. For larger Re, the detailed structure of the boundary layer is important for a considerable part of the motion. However, a simplifying feature is that, when the boundary layer must be modelled, the core flow need not be, since it is a simple plug flow. In either case, the small-time solutions (32)–(34) are used to start the numerical procedure. Because of the diffusive nature of the solution, a rather small time step is needed for the integration to be stable. For all Reynolds numbers, the velocity profile eventually becomes nearly parabolic and then fewer points are needed in the discretization of the x-direction. In the limit of parabolic flow, the central difference scheme is exact and only two points are needed to apply the boundary conditions. The error in these numerical solutions is estimated to be 0.1 % up to $t = 4$.

The solutions for $h(t)$, $h_t(t)$ and $\delta^*(t)$ are shown in figures 5, 6 and 7.

Figure 7 shows that the integral boundary-layer solution predicts δ^* very accurately up to the time when the boundary layers meet. The limit of validity of the integral solution $t_{\max}$ is predicted accurately for $Re \geqslant 10^3$, but overpredicted for smaller Re because then the boundary layers' development is not completed before they meet. The predictions of the displacement correction to h and h_t shown in figures 5 and 6 are accurate well beyond $t_{\max}$, because the total flow does not change very much until

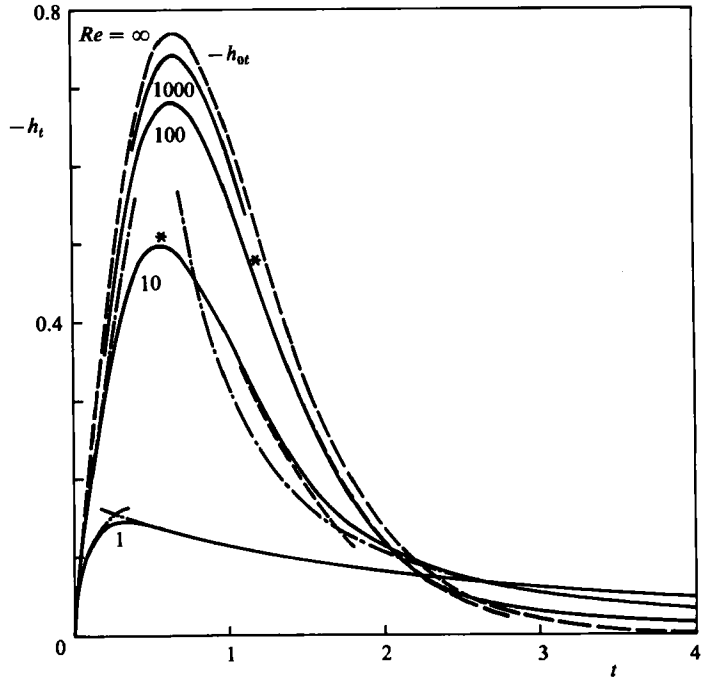

FIGURE 6. Solutions for the disk velocity $h_t(t)$: ——, numerical solution; – – – –, integral boundary-layer solution for large Re; *, predicted limit of large-Re solution; –·–·–·–, matched asymptotic solution for small Re.

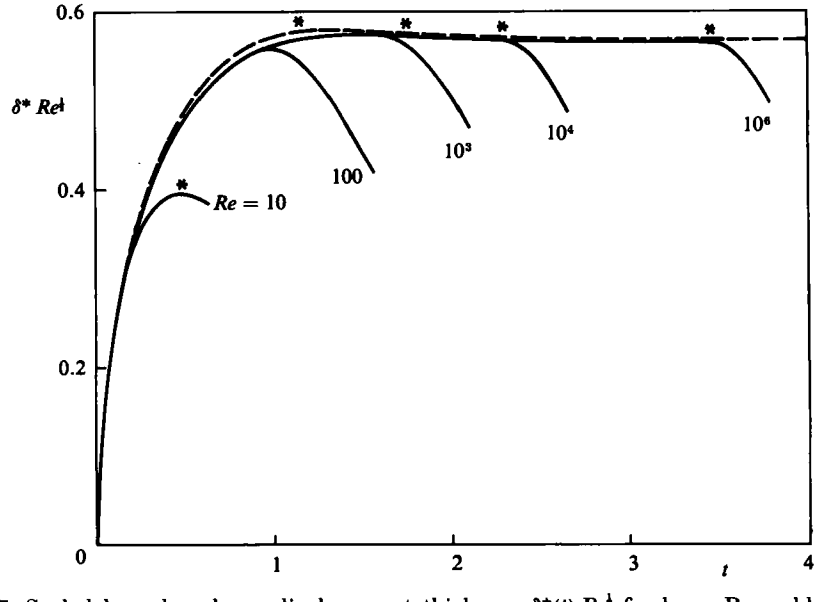

FIGURE 7. Scaled boundary-layer displacement thickness $\delta^*(t)\, Re^{\frac{1}{2}}$ for large Reynolds numbers: ——, numerical solution; – – – –, integral boundary-layer solution; *, predicted limit of validity of integral solution.

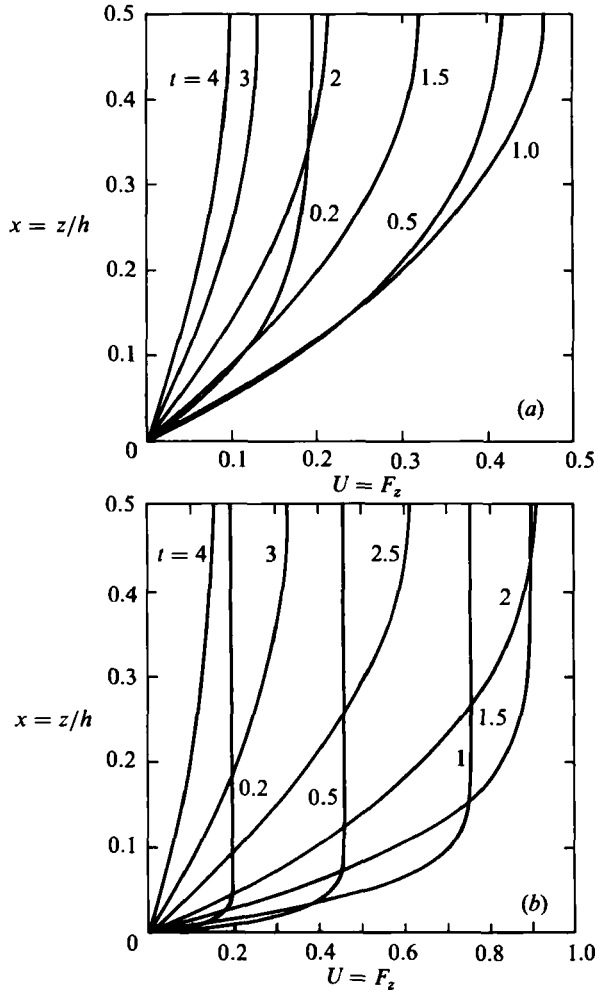

FIGURE 8. Development of radial-velocity profile with time: (*a*) $Re = 10$; (*b*) $Re = 1000$. Note that the velocity scale in (*a*) is twice that in (*b*).

well after the boundary layers meet. The figures indicate that the integral boundary-layer method gives satisfactory results for almost all of the motion for Re larger than 1000. For smaller Re, the boundary layers meet when the height is still relatively large and the interaction is important. The figures also confirm that the small-Re solution derived in Part 1 retains some accuracy up to a Reynolds number of 10.

The development of the velocity profile is shown in figure 8 for $Re = 10$ and $Re = 1000$. For the larger Reynolds number, the profile shows a boundary layer almost until the peak velocity is achieved. The boundary layers merge between $t = 1.5$ and 2.0 and then the viscous forces slow down the flow, with the profile moving towards a parabola. For the smaller Reynolds number, the viscous effects become important well before the peak velocity is achieved. The acceleration of the viscous flow is much slower and a lower maximum velocity is achieved.

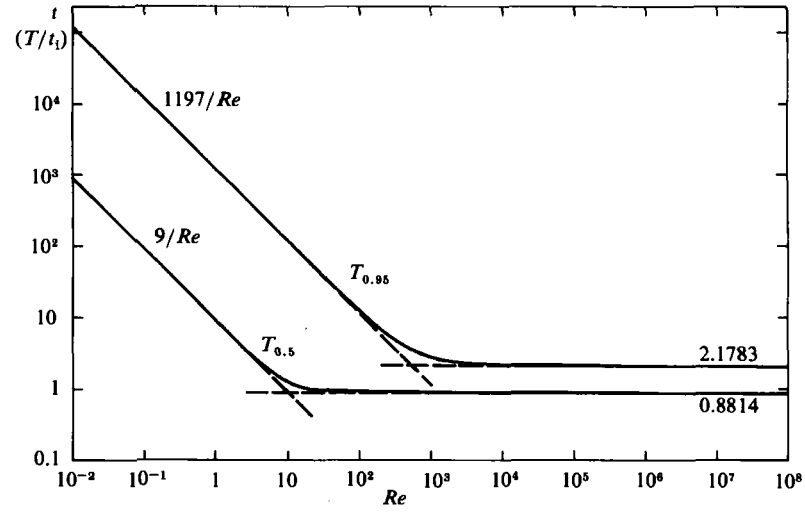

FIGURE 9. Draining times: T_f is the time for a fraction f of the fluid to drain from the gap.

Limit	Ordering of timescales	Draining time T
$Re \to \infty, \beta \to 0$	$t_g \ll t_i \ll t_d$	$2.18t_i$
$Re \to \infty, \beta \to \infty$	$t_i \ll t_d, \quad t_i \ll t_g$	$1.38t_g$
$Re \to 0, \beta \to 0$	$t_d \ll t_i, \quad t_g \ll t_i$	$1197t_v$

TABLE 1. Summary of results for dimensional draining time T in limiting cases

6. Discussion

Part 1 began with a discussion of the timescales involved in the problem and we are now in a position to resume that discussion. Figure 9 shows the times for the draining of 50 and 95% of the fluid-filled gap as a function of Reynolds number for zero β. The time for h to fall to 5% of its original value will be referred to as the draining time. We see that this is nearly constant for $Re > 10^3$, when the fluid motion is largely inviscid throughout the draining time. For smaller Re, viscous effects become important during the draining time and the time taken varies inversely with Re. This figure is plotted using a dimensionless time based on t_i. The results are more illuminating when put in dimensional form, with dimensional draining time T. For zero β, we have two limiting cases. For large Re ($\geqslant 10^3$), $T = 2.18t_i$, so the draining time is indeed characterized by the inertial time t_i. For small Re (< 10), $T = 1197t_v$, so the draining time depends only on t_v, but it is a very large multiple of t_v. This explains why the low-Reynolds-number analysis was valid even for Re up to 10. The results of all the limiting cases presented in the two papers can be treated in this way and are summarized in table 1.

The limit $Re \to 0, \beta \to \infty$, is not treated in the two papers, since only pathological physical interpretations could be found. The results in this limit depend on the size of the product $Re\beta$. The table confirms the interpretations of the three characteristic times of the problem and the limits in which they are important.

The draining time is determined by the dominant force resisting the motion. If the

fluid inertia is dominant, the draining time is characterized by t_i. If the viscous forces are dominant, the important timescale is t_v, but the draining time is a large multiple of t_v. This is because t_v is based on the initial configuration and the velocity decreases as the gap narrows. If the body inertia is dominant, the draining time is characterized by t_g.

REFERENCES

FRÖSSLING, N. 1940 *Lunds Univ. Arsskr. N. F. Afd.* 2, 35, no. 4.

WEINBAUM, S., LAWRENCE, C. J. & KUANG, Y. 1985 *J. Fluid Mech.* **156**, 463.